ELSEVIER

Journal of Photochemistry and Photobiology A: Chemistry 104 (1997) 13–18

Journal of PHOTOCHEMISTRY AND PHOTOBIOLOGY A:CHEMISTRY

Photodissociation dynamics of HNO_3 at 266 nm

Sun Jong Baek [a], Chan Ryang Park [b], Hong Lae Kim [a,*]

[a] *Department of Chemistry, College of Natural Sciences, Kangwon National University, Chuncheon, 200-701, South Korea*

[b] *Department of Chemistry, College of Natural Sciences, Kookmin University, Seoul, 136-702, South Korea*

Received 14 March 1996; accepted 6 November 1996

Abstract

The photodissociation dynamics of HNO_3 at 266 nm has been investigated by measuring laser induced fluorescence spectra of the $OH(^2\Pi)$ fragments. The measured fractions of the available energy distributed among the fragments are $f_t = 0.21$, $f_r(OH) = 0.047$, $f_{int}(NO_2) = 0.74$, and negligible OH fragments are found in the vibrationally excited states. By analyzing Doppler profiles of the spectra, vector correlations in the photodissociation of HNO_3 have been measured. The measured correlations show that the transition is parallel ($\beta_{\mu v} = 1.0$) but the transition dipole moment and the recoil velocity of the fragment are not exactly parallel. The rotational angular momentum J of the product OH is aligned parallel to the recoil direction of the fragment. From the measured correlations and the large fraction of the internal energy in the NO_2 fragments, it has been concluded that the transition at 266 nm is described as vibronic to the pyramidal excited state of A″ symmetry. Together with the measured Λ-doublet distribution of the OH fragments, the dynamics of photodissociation is discussed in detail. © 1997 Elsevier Science S.A.

Keywords: Photodissociation; Vector correlations

1. Introduction

Photochemical reactions are of fundamental importance to the detailed study of chemical reaction dynamics. Since the molecules of interest collide with photons having well-defined momenta, the theories are much simpler than those of reactive scattering events and applicable to even moderately large molecules [1–3]. The processes are governed by an initially prepared state and shape of potential energy surfaces along the reaction coordinate. An appropriate theory predicts the physical properties of final states, the physical observables of which are product distributions, energy distributions among various degrees of freedom of the products, and so forth. By examining the dynamics of the process, the shape of the potential energy surfaces can be studied in detail and thus the electronic structures of the molecules as well.

Spectroscopic transitions in molecules to the repulsive part of the potential energy surface result in continuous spectra. One can theoretically determine the energies and describe the nature of the transitions by ab initio calculations. When the dissociation starts from this repulsive potential surface, the angular distribution of the fragments is especially important among the many experimental observables in determining the nature of the photoprepared state. Maximum absorption of the dissociating light by the molecule takes place when the transition dipole moment of the molecule lies along the electric vector of the linearly polarized dissociating light. Thus, the angular distribution of the recoiling fragments measured relative to the electric vector of the dissociating light in the laboratory frame reveals the direction of the transition dipole moment of the molecule in the molecular frame. From the direction of the transition dipole moment, the symmetries of the excited state can be determined according to proper selection rules.

Studies of photodissociation dynamics in detail require precise measurements of certain physical properties related to potential energy surfaces. The population and energy distributions among the quantum states of the reactants and products are scalar properties from which the mechanism of photodissociation can be deduced. However, in most cases, measuring the energy distribution is not enough to study the detailed dynamics of the process. The transition dipole moment of the parent molecule, recoil velocities and rotational angular momenta of the products are vector properties of the molecule, and correlations between these vector properties reveal the detailed dynamics of the photodissociation. In order to measure the angular distribution and speed of the products, a rotatable time-of-flight mass spectrometer has been used [4]. In favorable cases such that the molecules of

* Corresponding author. Tel: +82 361 50 8492; fax: +82 361 53 7582.

PII S1010-6030(96)04563-7

interest absorb or emit photons of an easily accessible spectral region, Doppler resolved absorption or emission spectra provide the translational and internal energy distributions of the fragments. In addition, when linearly polarized lights are used for photolysis and probe, the vector correlations can be measured from the spectra by analyzing the Doppler profiles. The Doppler profiles in polarized absorption and emission spectra of molecules have been thoroughly analyzed by Herschbach and co-workers [5]. This Doppler spectroscopic technique is limited by the resolution of the spectra. The translational energies of the fragments should be large enough to provide broad spectroscopic transitions that should also be rotationally resolved in the spectra under the given resolution. A commercial pulsed dye laser currently available typically provides 0.04 cm^{-1} bandwidth in the visible region, and various laser spectroscopic techniques such as laser induced fluorescence (LIF) have been widely used to obtain the high resolution spectra of the photofragments [6,7]. The detailed photodissociation dynamics of OH-, NO-, and CN-containing molecules have been studied using this Doppler spectroscopy [8,9].

Studies of the photodissociation of HNO_3 by irradiation of UV light have been reported for many years. The absorption spectra in the UV show continuous absorption which peaks around 270 nm and 180 nm with increasing intensity [10]. The peaks have been assigned as $n \rightarrow \pi^*$ type transitions for both. Recent ab initio calculations predict the lower energy transition to be responsible for the π^* type excited states of A″ symmetry, while the higher energy transition is to the excited state of A′ symmetry assuming the parent molecule preserves the C_s symmetry [11,12]. However, by analyzing the Doppler profiles of the LIF spectra of the OH fragments produced from the photodissociation at 280 nm, Simons and co-workers found the transition dipole moment at this wavelength to lie parallel to the dissociating N–O bond axis, which implies that the excited state would be of A′ symmetry. They assumed a bent configuration on absorption and thus the transition would be vibronic as evidenced by large internal excitation of the NO_2 fragment [13,14]. Crim and co-workers studied a vibration-mediated two-photon and a single-photon dissociation at 241 nm [15]. They measured a smaller fraction of translational energies in the products than from longer wavelength dissociation, from which they concluded that the excited state at this wavelength is an A″ state which correlates to the ground state OH and NO_2 in its excited B state according to ab initio calculations. At 193 nm, the measured rotational energy distribution is cold and little vibrational excitation of OH has been found [16]. From the IR emission of NO_2 produced by photodissociation at 193 nm, Suto and Lee found large internal excitation in the NO_2 fragments [17]. In order to clarify the potential energy surfaces in detail in this energy region, the measurements of the angular distribution as well as the energy distribution among the fragments from the photodissociation at different wavelengths are of crucial importance.

The dissociation dynamics depends on the potential energy surfaces reached by the molecule on absorption of photons. Therefore, more studies on the complicated potential energy surfaces in this energy region are needed by precise measurements of the dynamical variables. In this study, the complete vector correlations in the photodissociation of HNO_3 at 266 nm have been measured by analyzing the Doppler profiles in the LIF spectra of OH. The measured correlations show that the transition is parallel. The fragment rotational angular momentum J lies parallel to the recoil direction, which suggests out-of-plane dissociation. Together with the measured Λ-doublet and energy distribution of the fragments, the dynamics of the dissociation is discussed in detail.

2. Experiment

The experiment was performed in a flow cell with conventional pump-probe geometry. The cell is a cube made of stainless steel with four arms in which baffles are placed to minimize scattered light. The cell was evacuated at about 10^{-3} Torr and gaseous HNO_3 was continuously flowed at a sample pressure of about 20 mTorr.

The horizontally polarized 266 nm dissociating light is obtained from the fourth harmonic of an Nd:YAG laser (Lumonics YM 800). The second harmonic of the same YAG laser separated from the 266 nm light through prisms pumps a tunable dye laser (Lumonics HD 500). The visible dye laser output is frequency doubled to probe OH by laser induced fluorescence employing the $A \leftarrow X$ transition in the UV region. The two laser beams are temporally separated by about 10 ns, which is measured by a fast photodiode. It is believed that the 10 ns delay of the probe from the pump and the 20 mTorr sample pressure should provide the nascent product energy distribution. The 0–0 transition in OH is employed and the total emission is probed without any filter in order to measure the correct intensity distribution. The powers of the two laser beams were kept as low as possible to minimize the scattered radiation, which is in turn discriminated with a gated integrator. The probe laser power is less than 20 μJ per pulse to avoid saturation as well. In order to measure the Doppler profiles, the 0–0 transition in OH is again employed and the $1 \leftarrow 0$ total emission is probed through a bandpass filter centered at 340 nm. The probe light is also horizontally polarized and the bandwidth is 0.06 cm^{-1} in the visible region, measured from the spectra of gaseous I_2 in a static cell at ambient temperature. In order to have two different pump-probe geometries, the dissociating and the probe lights are collinearly counterpropagated or the two laser beams are crossed at a right angle. The latter geometry (I) provides $\epsilon_d \perp k_p$ and $\epsilon_d \| \epsilon_p$, while the former (II) provides $\epsilon_d \| k_p$ and $\epsilon_d \perp \epsilon_p$ (Fig. 1), where ϵ_p and ϵ_d are the directions of the electric vectors of the linearly polarized probe and dissociating light, respectively, and k_p is the propagation direction of the probe light. More than two different experimental geometries are needed to measure the vector correla-

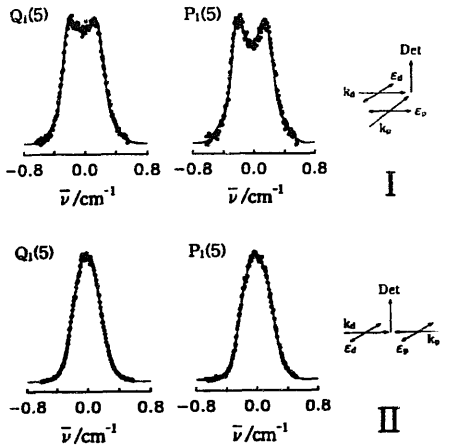

Fig. 1. Typical Doppler profiles of the OH spectra of the P- and Q-branch rotational transitions from the rotational state $N=5$ in the $OH(^2\Pi_{3/2})$ state under two different experimental geometries: (I) $\epsilon_d \perp \epsilon_p, \epsilon_d \| k_p$, and (II) $\epsilon_d \| \epsilon_p, \epsilon_d \perp k_p$.

tions discussed in the introduction. The detector is placed on top of the plane formed by the two laser beams.

The laser induced fluorescence is detected by a PMT (Hamammatsu R212UH) and the detected signal is fed to a boxcar averager. The powers of dissociating and probe laser lights were separately measured with photodiodes and the fluorescence signal is corrected with respect to the laser powers. A signal processor (EG&G 4420) digitizes the signal which is stored and processed in a PC.

3. Results and analyses

A portion of the LIF spectra of the OH products produced from the photodissociation of HNO_3 at 266 nm is presented in Fig. 2. The rotational transitions in the 0–0 band of the $A \leftarrow X$ transition are resolved and assigned according to Dieke and Crosswhite [18]. From the measured spectra, the rotational population distribution of the OH fragments are obtained from the reported Einstein B coefficients [19]. The

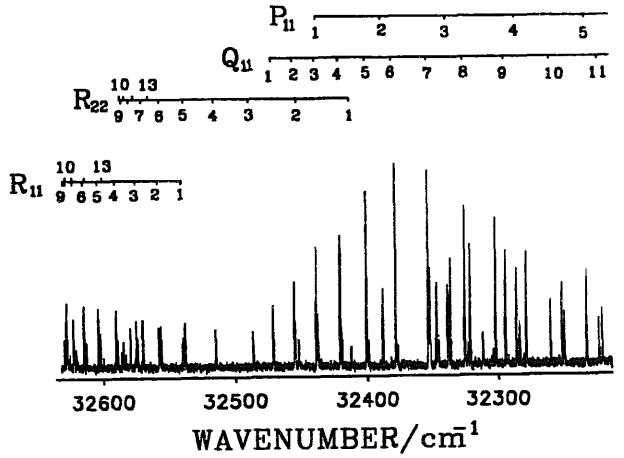

Fig. 2. A portion of the LIF spectra of OH produced from the photodissociation of HNO_3 at 266 nm employing the 0–0, A–X electronic transition. Rotational assignments are from Ref. [18].

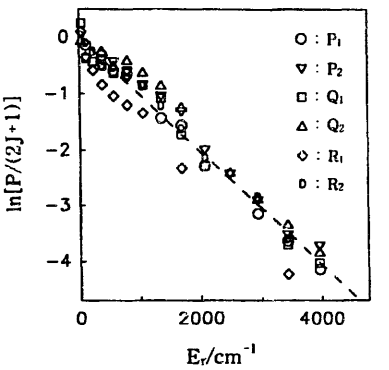

Fig. 3. Boltzmann plot of the rotational population distribution of CH obtained from the P-, Q-, and R-branch transitions in the $OH(^2\Pi_{3/2})$ and $OH(^2\Pi_{1/2})$ states.

rotational population peaks at $N=6, 7$ and extends to $N=14$. The rotational temperature is estimated to be about 1400 K assuming Boltzmann population distribution (Fig. 3) and the available energy distributed in the product OH rotation is found to be about 1000 cm^{-1} on average. The rotational transitions from higher vibrational states have such negligibly small intensities that the transitions could not be identified from the noise in the spectra. Thus, it has been concluded that the population of OH in the higher vibrational states is negligible.

Correlations of rotation with translational motion have been thoroughly analyzed by Dixon, and the anisotropy is defined by a number of bipolar moments of the translational and rotational angular distributions [5]. The Doppler broadened lineshape in the LIF spectra of the photofragments depends on the rotational alignment, polarization of the photolysis and probe laser lights, excitation–detection geometries, and the rotational branch transitions probed. The generalized lineshape functions are then given by

$$g(\chi_D) = \frac{1}{2\Delta v_D}[g_0 + g_2 P_2(\chi_D) + g_4 P_4(\chi_D) + g_6 P_6(\chi_D)]$$

where χ_D and v_D are the relative and the maximum Doppler shift, respectively, and P are the even-order Legendre polynomials. The Legendre polynomials of the fourth and sixth order are often neglected since the contribution of these higher-order terms to the Doppler profiles are small compared to the experimental errors. The multipliers, g, in the above equation are the linear combination of the bipolar moments β_0^k, which are given by

$$g_0 = b_0 + b_1 \beta_0^2(02)$$

$$g_2 = b_2 \beta_0^2(20) + b_3 \beta_0^0(22) + b_4 \beta_0^2(22)$$

where b can be calculated from the excitation–detection geometries and the angular momentum coupling factors defined by Dixon. In this experiment, two different excitation–detection geometries described in the experimental section have been employed, and the corresponding b values have been obtained for the different rotational branch transitions (Table 1). The bipolar moments $\beta_0^2(02)$, $\beta_0^2(20)$,

Table 1
Multipliers, b_i, obtained from the excitation–detection geometries and rotational angular momentum coupling factors defined by Dixon for different rotational branch transitions [5](b)

Rot.transition	Geometry	b_0	b_1	b_2	b_3	b_4
$Q_1(2)$	I	1.0250	−0.3639	2.0500	−0.9643	0.5510
	II	1.0250	0.8034	−1.0250	−0.9643	0.6122
$P_1(2)$	I	0.9950	0.4257	1.9900	1.0500	−0.6000
	II	0.9950	−0.7829	−0.9950	1.0500	−0.5143
$Q_1(5)$	I	1.0450	−0.4830	2.0900	−0.8962	0.5121
	II	1.0450	0.9038	−1.0450	−0.8962	0.6901
$P_1(5)$	I	0.9836	0.3708	1.9672	0.7761	−0.4435
	II	0.9836	−0.5198	−0.9836	0.7761	−0.2559
$Q_1(6)$	I	1.0464	−0.4974	2.0929	−0.8903	0.5087
	II	1.0464	0.9145	−1.0464	−0.8903	0.6968
$P_1(6)$	I	0.9821	0.3723	1.9642	0.7502	−0.4287
	II	0.9821	−0.4997	−0.9821	0.7502	−0.2335
$Q_1(9)$	I	1.0483	−0.5261	2.0967	−0.8822	0.5041
	II	1.0483	0.9337	−1.0483	−0.8822	0.7060
$P_1(9)$	I	0.9796	0.3799	1.9593	0.7080	−0.4046
	II	0.9796	−0.4710	−0.9796	0.7080	−0.1992

$\beta_0^0(22)$, $\beta_0^2(22)$ represent the rotational alignment, $\beta_{\mu J}$, translational anisotropy, $\beta_{\mu v}$ ($=2\beta_0^2(20)$), and v–J and μ–v–J photofragment vector correlations, β_{vJ} and $\beta_{\mu vJ}$, respectively. The experimental Doppler profiles are fitted by the equation

$$g(\chi_D)=\frac{1}{2\Delta v_D}[1+\beta_{eff}P_2(\theta)P_2(\chi_D)]$$

where θ is the angle between the recoil velocity and the probe direction and

$$\beta_{eff}=[b_2\beta_0^2(20)+b_3\beta_0^0(22)+b_4\beta_0^2(22)]/g_0P_2(\theta)$$

From a least-squares fit of the observed profiles to the above equation, the bipolar moments can be obtained by solving the linear equations.

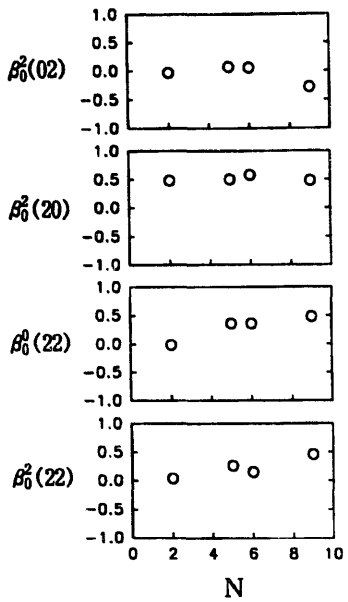

Fig. 4. Measured bipolar moments as a function of OH rotation.

The Doppler resolved spectra have been measured for the P_1 and Q_1 rotational branch transitions with the rotational angular momenta $N=2, 5, 6, 9$ which are well separated from other transitions. Since the NO_2 fragments have internal energy distributions, the OH fragments should have corresponding speed distributions. However, the internal energy distributions of the NO_2 fragments have not been measured in this experiment. Thus, the measured profiles were fitted assuming gaussian speed distributions with various widths. In order to find the best fits, the following procedure was employed. First, the best fit was found to the observed profile of one rotational transition varying β_{eff}, the average speed, and the width of the speed distribution. The measured average speed and the width for the best fit are 2100 m s^{-1} and 600 m s^{-1}, respectively. Then, for the profiles of different branch rotational transitions and the different experimental geometry at the same N, the best fit was found by just varying β_{eff}. The measured vector correlations from the observed Doppler profiles of different N are presented in Fig. 4. In this figure, the positive anisotropy parameter ($\beta_0^2(20)=0.5$) and the positive v–J correlation can clearly be seen with the slightly positive rotational alignment. This result implies the parallel transition to the A′ excited state with out-of-plane fragmentation, as mentioned in the Introduction. The μ–v–J correlation is also found to be positive, as expected when not all of the three vectors are perfectly parallel to each other.

In Fig. 5, the Λ-doublet distribution in the OH fragment is presented as a function of the rotational angular momenta N, while the statistical ratio is unity. The measured distribution shows that the A″ Λ-doublet state is preferentially populated, which suggests that the fragment OH tends to rotate in the plane perpendicular to the dissociating bond axis.

4. Discussions

The LIF spectra of OH from the photodissociation of HNO_3 at 266 nm have been obtained and the energy, Λ-doublet

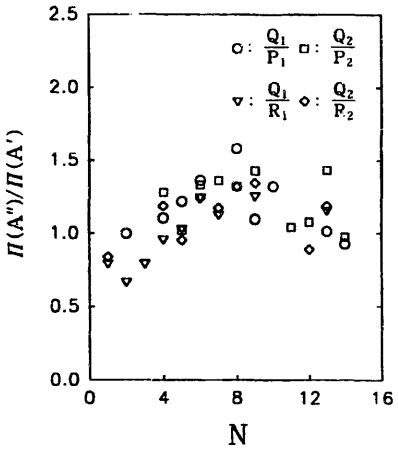

Fig. 5. Λ-doublet distribution of OH obtained from the Q-, P- and R-branch rotational transitions.

distribution and vector correlations of the fragments have been measured from the spectra.

The angular distribution measured from the Doppler profiles of the spectra ($\beta_{\mu v}=1.0$) suggests that the transition dipole moment at this wavelength should lie parallel to the dissociating N–O bond axis, and thus the excited state is expected to be of A′ symmetry. However, according to the recent ab initio calculation, the transitions in this energy region lead the parent molecule to the π^* type molecular orbitals that are of A″ symmetry [11,12]. The transition to this A″ state should result in the anisotropy parameter $\beta_{\mu v}$ being negative (-1 for the limiting case). The continuous absorption spectra appear to have two peaks in this energy region which are assigned to the three $\pi^* \leftarrow$ n transitions. The lower energy transitions are described by

(15a′) ^{1}A′ → (17″) 1^{1}A″

(14a′) ^{1}A′ → (17″) 2^{1}A″

and the excited state at the higher energy is of A′ symmetry. The transition to the A′ state occurs below 180 nm according to the calculation. Thus, the transition at 266 nm should be expected for the parent molecule to reach the A″ excited state according to the electronic selection rules. However, judging from the measured positive anisotropy parameter, the transition might be vibronic in this case. If the excited states are of π^* type molecular orbital character, the molecule in the excited state will be pyramidal as expected from the molecular orbital interactions. The transition then occurs through the a″ type out-of-plane bending vibrational motion, which results in overall A′ symmetry of the transition, and the positive anisotropy parameter is expected as observed. The angle between the transition dipole moment and the recoil velocity, $\theta_{\mu v}$, is related to the translational anisotropy, $\beta_{\mu v}$, which is given by $\theta_{\mu v}=\arccos(\frac{2}{3}\beta_{\mu v}+\frac{1}{3})^{\frac{1}{2}}$. The measured anisotropy is smaller than the limiting value. From the above equation, $\theta_{\mu v}$ is calculated to be about 35°, which implys that the HNO_3 in this excited state is pyramidal. The recent ab initio calculation by Bai and Segal indeed shows the angle between the NO_2 moiety and OH to be about 30° for the ^{1}A″ excited state [12]. Thus, it can be concluded that the transition at 266 nm still leads the parent molecule to the A″ excited state which was previously found and proposed by Simons and co-workers [13,14]. This vibronic transition should in turn result in a large internal excitation in the NO_2 fragment, as estimated in this experiment and discussed below.

The available energy that can be distributed among the fragments is the dissociation energy ($D_0=16\,720$ cm^{-1}) subtracted from the photon energy ($h\nu=37\,594$ cm^{-1}), and the average internal and translational energy of the parent molecule at ambient temperature (475 cm^{-1}). The available energy is then 21 350 cm^{-1}. The measured fractions of the available energy in the translation and internal degrees of freedom of the fragments are listed in Table 2. In general, if the dissociation taking place is fast along the repulsive potential energy surfaces, most of the available energy is likely to be transformed into the product translation, although this depends in part on the structure and lifetime of the excited molecule. However, as can be seen in the table, a large fraction of the available energy is in the internal motion of the NO_2 fragments, although the dissociation is fast enough for observation of the anisotropic angular distribution in the Doppler profiles. This is rationalized by the pyramidal excited structure as discussed above. In fact, emission from the excited NO_2 on photodissociation of HNO_3 at 193 nm shows the vibrationally excited NO_2 fragments [17].

Coupling of rotational and electronic orbital angular momenta produces two Λ-doublet fine structure states. In diatomic molecules with half-filled electronic orbitals such as OH, an electronic wavefunction of the unpaired electron is, in the limit of high rotation, approximated to the atomic orbital wavefunction which has definite symmetries with respect to the plane of molecular rotation. The symmetric wavefunction represented as a lobe in the plane of rotation is assigned to the A′ state among the two Λ-doublet components, while the antisymmetric wavefunction as a lobe perpendicular to the plane is assigned to the A″ state. These definite parities from rotational selection rules in electronic transitions such as P- and R-branch transitions should be induced form the A′ state and Q-branch transitions from the A″ state. Attention has long been paid to the Λ-doublet distribution because it reveals the planarity of the dissociation [20]. The repulsive force on dissociation and bending vibrational motion of the parent molecule should produce in-plane OH rotation which preferentially populates the A′ Λ-doublet component of OH, while torsional motion of the parent mol-

Table 2
Fractions of the available energy distributed in the products produced from the photodissociation of HNO_3 at 266 nm

E_{av} (cm^{-1})	$<f_t>$	$<f_r(OH)>$	$<f_v(OH)>$	$<f_{int}(NO_2)>$
21 350[a]	0.21	0.047	<0.01[b]	0.74

[a] $E_{av}=h\nu(266\text{ nm})+E(HNO_3\text{ at }300\text{ K})-D_0(OH\text{–}NO_2)$.
[b] Approximated from the noise in the spectra.

ecule should produce helical motion of the OH fragment, leading to out-of-plane dissociation and A″ propensity among the Λ-doublet distribution in OH. The measured Λ-doublet distribution shows a propensity in the A″ state and then no propensities at higher N (Fig. 5). The atomic orbitals for the unpaired electron in the OH fragments formed during the dissociation appear to lie along the dissociation axis perpendicular to the plane of the molecular rotation. The rotation of OH mainly originates from the parent torsional motion and the bending vibration of the parent molecule becomes significant at higher N. Simons and co-workers discussed the dependence of the v–J correlation on the rotational angular momenta of OH in their 280 nm dissociation of HNO_3 [14]. In order to explain the experimental results, they proposed another dissociation channel which generates the NO_2 in the B state with an increased bending torque, but in the present experiment such a conclusion is not unambiguous.

In addition to the A″ propensity in the Λ-doublet distribution, the measured positive v–J correlation suggests out-of-plane dissociation. The fraction of photofragments with $v \| J$ and $v \perp J$ is related to the v–J correlation, which is given by $f(\|) = \frac{1}{3}(1 + 2\beta_{vJ})$ and $f(\perp) = \frac{1}{3}(1 - \beta_{vJ})$, respectively. The measured v–J correlation reveals that about 70% of the fragments are generated with $v \| J$, suggesting that torsional motion plays an important role in the OH fragment rotation. If the transition dipole moment, recoil velocity, and rotational angular momenta are all perfectly parallel to each other, then the resulting μ–v–J correlation has a limiting value of -1, while any one perpendicular to the other two provides the positive limiting value. The measured positive μ–v–J correlation, which is even smaller than the limiting value, and the slightly positive rotational alignment indicate that the recoil velocity and the transition dipole moment are not parallel.

In summary, the absorption of photons at 266 nm by HNO_3 leads the molecule to the $1^1A''$ excited state via the vibronic transition. The structure of the molecule in this excited state is pyramidal, from which the dissociation is fast and directly generates the OH and NO_2 fragments in the ground electronic state. The recoiling OH fragment is rotating in the plane perpendicular to the dissociating axis (out-of-plane dissociation), whose rotational motion mainly originates from the torsional motion of the parent molecule.

Acknowledgements

This work has been supported by the Korea Science and Engineering Foundation (95-0501-13-3) and the Ministry of Eduacation of Korea.

References

[1] S.J. Singer, K.F. Freed, Y.B. Band, Adv. Chem. Phys. 61 (1985) 1.
[2] R. Schinke, Photodissociation Dynamics, Cambridge University Press, 1993.
[3] M.N.R. Ashfold, J.E. Baggott (Ed.), Molecular Photodissociation Dynamics, Royal Society of Chemistry, London, 1987.
[4] S.J. Riley, K.R. Wilson, Faraday Discuss. Chem. Soc. 53 (1972) 132.
[5] (a) R.N. Zare, D.R. Herschbach, Proc. IEEE 51 (1963) 173.(b) R.N. Dixon, J. Chem. Phys. 85 (1986) 1866.
[6] W. Demtroeder, Laser Spectroscopy, Springer, Berlin, 1982.
[7] J.M. Hollas, High Resolution Spectroscopy, Butterworth, London, 1982.
[8] G.E. Hall, P.L. Houston, Ann. Rev. Phys. Chem. 40 (1989) 375.
[9] P.L. Houston, J. Phys. Chem. 91 (1987) 5388.
[10] H. Johnston, R. Graham, J. Phys. Chem. 77 (1973) 62.
[11] L.E. Harris, J. Chem. Phys. 58 (1973) 5615.
[12] Y.Y. Bai, G.A. Segal, J. Chem. Phys. 92 (1990) 7479.
[13] J. August, M. Brouard, J.P. Simons, J. Chem. Soc., Faraday Trans. 84 (1988) 587.
[14] M. Brouard, S. Duxon, P.A. Enriquez, J.P. Simons, J. Chem. Soc., Faraday Trans. 89 (1993) 1435.
[15] A. Sinha, R.L. Vander, F.F. Crim, J. Chem. Phys. 91 (1989) 2929.
[16] A. Jacobs, K. Kleinermanns, H. Kuge, J. Wolfrum, J. Chem. Phys. 79 (1983) 3162.
[17] M. Suto, L.C. Lee, J. Chem. Phys. 81 (1984) 1294.
[18] G.H. Dieke, H.M. Crosswhite, J. Quant. Spectrosc. Radiat. Transfer 2 (1962) 97.
[19] I.L. Chidsey, D.R. Crosley, J. Quant. Spectrosc. Radiat. Transfer 23 (1980) 187.
[20] I. Hanazaki, Chem. Phys. Lett. 201 (1993) 301.